

Coarse-grained spectral projection (CGSP): A scalable and parallelizable deep learning-based approach to quantum unitary dynamics

Pinchen Xie

*Program in Applied and Computational Mathematics,
Princeton University, NJ 08544, USA*

Weinan E

*Department of Mathematics and Program in Applied and Computational Mathematics,
Princeton University, NJ 08544, USA*

(Dated: November 29, 2021)

We propose the coarse-grained spectral projection method (CGSP), a deep learning approach for tackling quantum unitary dynamic problems with an emphasis on quench dynamics. We show CGSP can extract spectral components of many-body quantum states systematically with highly entangled neural network quantum ansatz. CGSP exploits fully the linear unitary nature of the quantum dynamics, and is potentially superior to other quantum Monte Carlo methods for ergodic dynamics. Practical aspects such as naturally parallelized implementations on modern deep learning infrastructures are also discussed. Preliminary numerical experiments are carried out to guide future development of CGSP.

I. INTRODUCTION

The past several decades have witnessed a rapid growth of research interests in dynamical quantum many-body systems and hatched a series of remarkable experimental techniques [1–5] for manipulating and observing quantum matters. These developments led to the observation of novel quantum phenomena [6–10] outside the scope of equilibrium physics, and also opened the possibility for realistic implementations of quantum computations [11–15]. To further explore these topics, advanced numerical algorithm for simulating the dynamics of quantum many-body systems is highly desired. The purpose is not only observing and verifying theoretical findings, but also actively searching for new physical mechanisms or strategies to guide the design and the control of artificial quantum systems [16–26].

But unfortunately, the simulation of generic quantum dynamic problems usually brings out exponential complexity that is out of reach for classical computers. The major difficulty comes from the presence of high-dimensional highly-entangled quantum states during time evolution, which is, however, a guarantee of quantum advantages in quantum computation [27]. That being said, high-fidelity quantum simulation algorithms are immature, if not impossible, to be implemented at the current noisy intermediate-scale stage of quantum computing research [28], considering the tremendous resources demanded by error correction [29]. Therefore it is still of utter importance to continue pushing the limit of classical algorithms towards specialized quantum dynamic problems that are potentially accessible to classical computers.

To distinguish classically tractable quantum dynamic problems from the others, quantum entanglement and locality of the Hamiltonian serve frequently as practical criteria. The former is used to evaluate the quality of a

classical ansatz for representing high-dimensional quantum many-body states, while the latter determines the complexity of a classical algorithm for capturing quantum dynamics.

Quantum entanglement is at the heart of most tensor network ansatz originated from the density matrix renormalization group (DMRG) method [30]. Famous examples include Matrix product states (MPS), projected entangled pair states (PEPS) and multiscale entanglement renormalization ansatz (MERA) [31–33]. The usage of these ansatz is usually restricted to quantum states featuring area-law entanglement ($S < c \cdot \text{Area}$) with or without logarithmic correction [34, 35], a property commonly seen in low-lying states of many-body models with local interactions. However, except for some special cases such as many-body localization, a quantum dynamic system usually goes through many-body states with volume law entanglement. Even for a time evolution process starting from an unentangled initial state, the bipartite entanglement entropy of a quantum system can grow linearly towards saturation value (proportional to half system size), resulting in an exponential growth of the tensor network ansatz complexity. Therefore, the simulation of quantum dynamics is longing for more sophisticated classical ansatz as successor to tensor networks. In recent years, the most promising candidate turned out to be artificial neural networks which are capable of modeling highly-entangled quantum states [36]. An early practice along this line of research was the application of restricted Boltzmann machine (RBM) in solving the ground state and the dynamics of quantum spin models [37]. Later, symmetry preserving deep fully-connected neural networks (FNN) and convolutional neural networks (CNN) were also shown to be efficient quantum state ansatz [38–42]. In particular, CNN is believed to support volume-law entanglement scaling while being polynomially more efficient in resources compared to RBM-like ansatz in 2D, due to an inherent reuse of information [43].

While entanglement capacity poses a challenge to classical ansatz, the locality of Hamiltonian has made it possible for many classical algorithms to succeed. Examples include DMRG, time-evolving block decimation (TEBD) and time-dependent variational principle. Locality, or more generally sparsity in the linear algebra point of view, is outstanding in quantum lattice models with only short-range interactions like Hubbard model and Heisenberg models, allowing the numerical modelings of very large systems. On the contrary, the lack of sparsity in second quantized molecular Hamiltonians limits the scalability of accurate ab-initio methods like DMRG and variational Monte Carlo (VMC) in quantum chemistry [44].

Considering both high entanglement capacity and sparsity, the most promising classical algorithm for simulating real time quantum unitary dynamics is now time-dependent variational principle methods based on neural network ansatz (TDVP-NN) [37]. TDVP-NN projects real-time quantum evolution trajectory in the entire Hilbert space into a tiny useful subset, parameterized by a neural network, of the Hilbert space. The projected dynamics is then described by a low-dimensional time-dependent differential equation of neural network parameters. In spite of numerical instability of the projected dynamics and the limited expressive power of the neural network, this method is potentially capable of simulating quench dynamics of very large quantum spin systems with strong entanglement [45], ultrafast dynamics [46] and the evolution of open quantum systems [47].

However, the generality of TDVP-NN means that it does not give special treatment to dynamics driven by static Hamiltonians, slowly varying Hamiltonians or piecewise time-dependent Hamiltonians. Hence the propagation time step in TDVP-NN lacks the flexibility enjoyed by global Krylov-subspace-based methods. The reason is that the unitary structure of a single Hamiltonian and the spectral information of the initial condition are left unexplored.

In this work, we will show how to actually poke into the spectral structure of an evolving quantum state and extract limited but useful high-dimensional information. This is done through a coarse-grained representation of the spectral projection using deep neural networks. We will focus on quantum unitary dynamics driven by Hamiltonians with a sparse matrix representation in the trivial orthogonal basis. Many interesting problems can be found in this category, including the quench dynamics of Heisenberg model or a sparsely connected quantum circuits. The idea behind the approach we are trying to develop is conceptually similar to normal-mode propagation used in path-integral molecular dynamics simulation.

This paper is organized as follows. In Sec. II we introduce the concept of coarse-grained spectral projection (CGSP) and its possible application in quantum dynamics as a numerical tool. In Sec. III we propose a parallelized deep learning framework for practical CGSP with numerical experimental results.

II. COARSE-GRAINED SPECTRAL PROJECTION OF QUANTUM STATES

The high-dimensional nature of the Hilbert space of the quantum states has hindered the direct decomposition of quantum Hamiltonians or complete spectral projection of a quantum state. This also limits the feasibility of any supervised learning-based methodology that relies on data from exact diagonalization. On the other hand, note that the underlying eigen-frequency scale of a short-ranged Hamiltonian increases only linearly with respect to system size. This special property motivates the coarse-grained spectral projection approach that we are going to introduce.

Formally, a complete eigen-decomposition of a pure quantum state Ψ_o associated to a closed system Hamiltonian H can be expressed as

$$\Psi_o = \sum_{i=1}^{N_h} b_i \psi_i, \quad (1)$$

Here the eigenstates $\{\psi_i\}$ satisfy $H\psi_i = E_i\psi_i$. They are orthonormal and increasingly ordered with respect to the energy level E_i . N_h is the dimension of the Hilbert space \mathcal{H} .

There exist trivial disjoint cover of the entire energy spectrum on the real axis:

$$[E_1, E_{N_h}] \subset [x_0, x_1) \cup [x_1, x_2) \cup \cdots \cup [x_{N-1}, x_N] \quad (2)$$

such that $x_0 < E_1 < x_1 < x_2 < \cdots < x_{N-1} < E_{N_h} < x_N$. Without loss of generality, we assume $x_{i+1} - x_i$ is constant for all the intervals.

For each interval $[x_i, x_{i+1}]$ we associate the direct sum of the eigen-subspaces whose eigenvalues lie in $[x_i, x_{i+1}]$, we obtain N subspace $\{Q_i \in \mathcal{H}\}$ and N corresponding projection operators $\{\mathcal{P}_i\}$ for the N intervals.

Since $\mathcal{H} = \cup_{i=0}^{N-1} Q_i$, it is obvious that

$$\Psi_o \in \text{span}(\mathcal{P}_0\Psi_o, \cdots, \mathcal{P}_{N-1}\Psi_o). \quad (3)$$

Let θ_i denote the normalized $\mathcal{P}_i\Psi_o$. Ψ_o can be expressed as

$$\Psi_o = \sum_{i=0}^{N-1} c_i \theta_i. \quad (4)$$

Let $\epsilon = x_{i+1} - x_i$ and $\lambda_i = (x_i + x_{i+1})/2$ be the center of the i -th interval. The unitary evolution of $\Psi_o(t) = e^{-iHt}\Psi_o$ driven by time-independent Hamiltonian H can be approximated by

$$\phi_o(t) = \sum_{i=0}^{N-1} c_i e^{-i\lambda_i t} \theta_i. \quad (5)$$

The error has an evident upper bound

$$|\Psi_o(t) - \phi_o(t)| \leq \frac{\epsilon t}{2}. \quad (6)$$

It is clear that the number of energy intervals needed to achieve $|\Psi_o(t) - \phi_o(t)| < \delta$ for small enough δ grows only linearly with respect to t and the spectrum range, as indicated by

$$N > \frac{(E_{N_h} - E_1)t}{2\delta}. \quad (7)$$

Notice that the energy spectrum range $(E_{N_h} - E_1)$ usually grows linearly with system size for quantum models defined on (nearly) regular graphs with bounded short-range interaction and disorder. Recently, a similar bound has also been derived in the context of quantum state compression via principle component analysis [48].

Ideally, the projected states θ_i can be parameterized and solved by N classical ansatz. However, this is a difficult task for traditional ansatz with only area-law entanglement capacity. To the best of our knowledge, no classical algorithm has been developed yet. In this work, we will show that tools from deep learning can be borrowed to crack the volume law barrier imposed by entanglement. We will develop a data-free approach to quantum dynamics based on the ideas illustrated above. Instead of learning each unique θ_i accurately with neural networks, we can allow each θ_i to make some errors and that will not destroy the overall accuracy for approximating the dynamics.

Before going into specific details, let us make several compromises regarding the splitting of energy spectrum and the error estimates. First, given a disjoint cover of the energy spectrum like Eq. (2), it is nearly impossible to represent all unique projected states θ_i accurately with neural networks for large quantum systems. Thus the uniqueness condition should be loosened by allowing polluted projection.

With an abuse of notation, we re-assume a non-exact cover of the spectrum:

$$[E_1, E_{N_h}] \subset [x_0, y_0] \cup [x_1, y_1] \cup \dots \cup [x_{N-1}, y_{N-1}] \quad (8)$$

such that $x_i < x_{i+1}$ and $y_i < y_{i+1}$ holds for all $i \in [0, N-1]$. With this cover, the N subspace $\{Q_i \in \mathcal{H}\}_{i \in [0, N-1]}$ (and the N corresponding projection operators $\{\mathcal{P}_i\}_{i \in [0, N-1]}$) are still well-defined but they are not necessarily orthogonal to each other. So there exists non-unique N normalized states $\theta_i \in Q_i$ such that

$$\Psi_o = \sum_{i=0}^{N-1} c_i \theta_i. \quad (9)$$

Now θ_i is not necessarily the normalized $\mathcal{P}_i \Psi_o$ but only an element in Q_i . Obviously, $\{\theta_i\}$ can be non-orthogonal. Let $\lambda_i = \frac{\langle \theta_i | H | \theta_i \rangle}{\langle \theta_i | \theta_i \rangle}$, $\Psi_o(t)$ can again be approximated by $\phi_o(t) = \sum_{i=0}^{N-1} c_i e^{-i\lambda_i t} \theta_i$. The quality of this approximation is reflected by the ‘‘covariance’’ matrix

$$(M)_{ij} = \langle \theta_i | (H - \lambda_i)(H - \lambda_j) | \theta_j \rangle. \quad (10)$$

For small t , the error of the approximation is

$$|\Psi_o(t) - \phi_o(t)|^2 \approx t^2 \mathbf{c}^\dagger M \mathbf{c}. \quad (11)$$

In practice, it is easier to only calculate the diagonal element of M , i.e. the variance $\sigma_i^2 = \langle \theta_i | (H - \lambda_i)^2 | \theta_i \rangle$ of each θ_i . Let $|\sigma| = \max(\{\sigma_i\}_{i \in [0, N-1]})$. We have a very rough but inexpensive estimation of the error:

$$|\Psi_o(t) - \phi_o(t)| \approx |\sigma|t. \quad (12)$$

The error is systematically reducible when $|\sigma|$ scales as $1/N$. To achieve this goal within the framework of deep learning, we introduce N neural network ansatz Θ_i to represent the N normalized states θ_i respectively. The N neural network ansatz will sum up to the initial state Ψ_o . In addition, there should be an optimization scheme to minimize the variance σ_i of each neural network ansatz such that $|\sigma|$ is improvable. Therefore, we propose the following objective function as a constrained optimization problem:

$$\begin{aligned} & \text{minimize} \quad \sum_{i=0}^{N-1} c_i^2 \langle \Theta_i | (H - \Lambda_i)^2 | \Theta_i \rangle, \\ & \text{subject to} \quad d(\Psi_o(0), \sum c_i \Theta_i) = 0, \end{aligned} \quad (13)$$

Here the amplitude coefficients c_i and all network parameters of Θ_i are to be optimized. d can be any legal distance function in the Hilbert space including the Fubini-Study metric and L_2 norm, regardless of $U(1)$ symmetry. The fixed constants $\{\Lambda_i\}$ in the objective function is an arithmetic sequence satisfying $\Lambda_0 < E_{min}$ and $\Lambda_{N-1} > E_{max}$, with a common increment of $\epsilon > 0$. The ground state energy E_{min} of the system Hamiltonian and the maximum energy E_{max} can be easily estimated by usual VMC techniques with the same neural network ansatz. Notice instead of minimizing the variance directly, we choose to minimize a weighted sum of individual variances. We show in Appendix A that this particular choice of objective function leads to a N^{-1} scaling of $|\sigma|$. A practical algorithmic implementation of this optimization task is illustrated in Sec. (III) where auto-regressive generative neural networks [49] are used for quantum state ansatz and efficient Monte-Carlo sampling at the same time. In addition, considering the simultaneous optimization of many neural networks is hazardous, we propose a hierarchical framework in Sec. (III) to break Eq. (13) down into smaller, easily parallelizable optimization tasks from low to high spectral resolution.

When $N \rightarrow \infty$, Eq. (13) converges to its continuous form:

$$\begin{aligned} & \text{minimize} \quad \int_{w_a}^{w_b} c^2(w) \langle \Theta(w) | (H - w)^2 | \Theta(w) \rangle dw, \\ & \text{subject to} \quad d(\Psi_o(0), \int_{w_a}^{w_b} c(w) \Theta(w) dw) = 0. \end{aligned} \quad (14)$$

For many disordered system, eigenstates with very close energy levels can have completely different local observables [50]. Hence a global minimizer $\Theta_m(w)$ of Eq. (14) is

not expected to be continuous with respect to w . Therefore we adopt the discrete form Eq. (13) as the starting point for extracting spectral information and name it “coarse-grained spectral projection (CGSP)”.

Ideally, Eq. (13) provides a route to systematically improvable classical algorithms for simulating quantum dynamics after a sudden quench. Because deep neural network is used, the minimizer of Eq. (13) may be parameterized with only polynomial complexity. However, like all other classical algorithms, the precious polynomial complexity is conditional. In the following, we are going to compare CGSP with major quantum dynamics algorithms and analyze their pros and cons.

First of all, it is well known that tensor network ansatzs like matrix product states sacrifice entanglement capacity for general representation of many-body states with nearly area-law entanglement. The area-law constraint is so strong that tensor networks can cover almost all eigenstates for some models [51]. This makes TDVP-based evolution of tensor networks very stable and accurate in the weakly-entangled regime but ineffective otherwise.

However, when we consider TDVP-based evolution of neural networks for generic quantum dynamics, there is no comfort zone like weakly-entangled regime. High entanglement capacity of neural networks is a reward but not a permit to every corner of the many-body Hilbert space. After all, only a low-dimensional tiny section of the Hilbert space can be parameterized by a finite-size classical ansatz. Thus, for TDVP methods, the failure of polynomial complexity appears when the actual quantum state trajectory travels away from the low-dimensional section or encounters singular points of the ansatz. This failure is inevitable for ergodic dynamics harnessed by few symmetries. From an intuitive perspective, this phenomenon may be more easily perceived in quench dynamics over criticality [52].

For our CGSP method, the breakdown of polynomial complexity happens in a different situation. First, notice that in CGSP, the neural network is expected to parameterize only $O(t)$ many quantum many-body states. So, the burden on classical ansatz in CGSP is a countable finite subset of many-body Hilbert space, rather than a differentiable subset containing the real-time evolution trajectory. This statement holds true, regardless of ergodicity, for finite-time dynamics driven by time-independent Hamiltonian. Nevertheless, when t is large, even a countable finite subset of Hilbert space is too difficult for neural networks to represent fully. This is when CGSP will fail.

Based on the discussion above, it is clear that CGSP has a lighter burden to bear for quench dynamics, with only a $O(t)$ scaling factor on top of the complexity of ground states represented in the ansatz. However, from the optimization perspective, CGSP requires much more training efforts compared to TDVP-NN which propagate in a deterministic way when Monte Carlo sampling is nearly exact. Note that the optimization of a CGSP task is non-convex towards the objective Eq. (13). This means, like almost every deep learning task, CGSP may

suffer from local optimum and ill-conditioning. These issues will be addressed in detail in our future work.

We now discuss how to improve the TDVP simulation of quantum dynamics driven by slow-varying time-dependent Hamiltonian $H(t)$ with CGSP. Suppose the initial state $\Phi_o(0)$ has already found its CGSP representation $\Phi_o(0) = \sum_{i=0}^{N-1} c_i \theta_i$ with $\lambda_i = \frac{\langle \theta_i | H(0) | \theta_i \rangle}{\langle \theta_i | \theta_i \rangle}$. By allowing the parameters of the neural networks to be time-dependent and identifying θ_i as $\theta_i(t=0)$, a new ansatz can be defined using $\eta_i(t) = \theta_i(t)e^{-i\lambda_i t}$. Theoretically, if $\eta_i(t)$ evolves under the Schrödinger equation, then $\sum_{i=0}^{N-1} c_i \eta_i(t)$ is identical to $\Phi_o(t)$. So the evolution of $\eta_i(t)$ should satisfy the following time-dependent variational principle:

$$\delta \int_0^t \|i \frac{d\eta_i(s)}{ds} - H(s)\eta_i(s)\|^2 ds = 0, \quad (15)$$

which can be translated into

$$\text{minimize}_{\theta_i(t)} \|i \frac{d\theta_i(t)}{dt} - (H(t) - \lambda_i)\theta_i(t)\|. \quad (16)$$

Assume that the Hamiltonian is slowly varying and the spectral norm $\|dH(t)/dt\|_s$ is bounded by $B > 0$. Then one has

$$\| \frac{d\theta_i(t)}{dt} \| < Bt + \|(H(0) - \lambda_i)\theta_i(t)\| \quad (17)$$

If the CGSP is successful, one expects $\|(H(0) - \lambda_i)\theta_i(t)\| \ll 1$ for t small enough. Eq. (17) suggests how CGSP may help with TDVP-based simulation. For the plain TDVP approach, the variation of the ansatz $\|\frac{d\Psi(t)}{dt}\|$ is bounded by $\|H(t)\|_s \gg B$. For lattice models $\|H(t)\|_s$ usually grows linearly with system size. This means the differentiable manifold that the neural network should parameterize grows rapidly for ergodic dynamics. However, with CGSP-initialized TDVP simulation, the desired expressive power of the neural network grows much slower due to the constraint Eq. (17).

III. A HIGHLY PARALLELIZED APPROACH TO CGSP

To show that Eq. (13) is applicable to real quantum dynamic problems, we will propose a practical framework for using Eq. (13) in quench dynamics of quantum lattice models. In this framework, penalty method is used to establish an unconstrained optimization target and Monte Carlo is used to estimate the gradient. Recently developed neural autoregressive quantum states (NAQS) [49] will serve as the classical ansatz for boosted importance sampling. In addition, a parallel scheme is introduced for work-breakdown in high performance computing. The main purpose of this section is to provide a modularized framework for large-scale CGSP implementation that allows for potential improvement of the models and fast deployment with modern deep learning frameworks such as PyTorch and Tensorflow [53, 54].

A. Generative classical ansatz that boosts stochastic sampling

First, we introduce the basic ideas of NAQS. Unlike other neural quantum states with sophisticated VMC ansatz, NAQS can greatly boost the efficiency of stochastic importance sampling. Before NAQS, the popular sampling tool accompanying neural quantum states is Markov-Chain Monte-Carlo (MCMC), a default tool of VMC. Though parallelizable to some extent, MCMC is essentially a sequential algorithm, which is incompatible to large-scale deep learning applications using graphics processing units (GPUs). On the contrary, NAQS implements importance sampling in a parallel manner.

A NAQS is by default a normalized wave function that can be expressed as a product of normalized conditional wave function. For example, in the usual S_z basis of quantum lattice problems, a NAQS is expressed as

$$\Psi(s_1, \dots, s_l) = \prod_{i=1}^l \psi_i(s_i | s_{i-1}, \dots, s_1) \quad (18)$$

where $\psi_i(s_i | s_{i-1}, \dots, s_1)$ satisfies a local normalization condition $\sum_{s_i} |\psi_i(s_i | s_{i-1}, \dots, s_1)|^2 = 1$. It has been shown that a NAQS satisfying Eq. (18) can generate configurations $\{(s_1, \dots, s_l)\}$ directly according to the probability distribution $|\Psi(s_1, \dots, s_l)|^2$, with a higher sampling quality than MCMC [49].

At first glance, obtaining a mathematical structure indicated by Eq. (18) would require a sequence of neural networks. However in practice, the desired structure can be achieved easily in a parallel manner with masked convolutions. Successful realization of such structure has been published in many areas [55–57]. Moreover, it is quite straightforward to define charge conservation in NAQS: one only needs to mute these $\psi_i(s_i | s_{i-1}, \dots, s_1)$ associated to illegal configuration before enforcing local normalization condition. In our implementation of NAQS, we basically followed the design of WaveNet [55], of which the network depth scales with the logarithm of system size.

B. Loss function

The target Eq. (13) can be approached as an unconstrained optimization problem by defining the loss function

$$\begin{aligned} L = & \|\Psi_o(0) - \sum c_i \Theta_i\|^2 + \eta_1 \sum_{i=0}^{N-1} c_i^2 \langle \Theta_i | (H - \Lambda_i)^2 | \Theta_i \rangle \\ & + \eta_2 \sum_{|i-j| < r} \|\langle \Theta_i | \Theta_j \rangle\|^2, \end{aligned} \quad (19)$$

where $\eta_1, \eta_2 < 1$ are constant weights decaying over time. r is the fixed radius we choose for enhancing orthogo-

nalinity, $\{c_i\}$ and the parameters of all Θ_i are real variables. The fidelity term $L_{fid} = \|\Psi_o(0) - \sum c_i \Theta_i\|^2$ is the main term in this loss function. The orthogonality penalty term $L_{otg} = \eta_2 \sum_{|i-j| < r} \|\langle \Theta_i | \Theta_j \rangle\|^2$ is introduced to reduce projection pollution, i.e. the spill over to other subspaces that it should not belong. The second term $L_{var} = \eta_1 \sum_{i=0}^{N-1} c_i^2 \langle \Theta_i | (H - \Lambda_i)^2 | \Theta_i \rangle$ will be called the variance loss. Notice that without the orthogonality penalty, the variance is already suffice to enforce the N^{-2} scaling of $\sigma_i^2 = \frac{\langle \Theta_i | (H - \Lambda_i)^2 | \Theta_i \rangle}{\langle \Theta_i | \Theta_i \rangle}$ as explained in Appendix A. The orthogonality penalty is added only to further reduce σ_i without affecting the theoretical scaling behavior.

To parameterize all Θ_i , N neural networks are needed. In addition, the N networks are expected to run in parallel.

Unlike tensor-network-based ansatz, neural network states require Monte Carlo methods (mostly importance sampling) to estimate the inner product on Hilbert space. For NAQS, there are extra requirements when multiple wave functions are involved in importance sampling. One restriction is that the proposal distribution to be sampled has to be a sum of squared norm of wave function instead of the squared norm of a sum of wave function. For example, given two spin NAQS $X[s]$ and $Y[s]$, $|X[s]|^2 + |Y[s]|^2$ can be sampled directly while $|X[s] + Y[s]|^2$ can not.

Therefore, one has to carefully design proposal distributions for each term of the loss function. A natural choice towards variance reduction of each $\langle \Theta_i | (H - \Lambda_i)^2 | \Theta_i \rangle$ is the probability density of spin configuration $|\Theta_i[s]|^2$ (s is any spin configuration). For the fidelity term, out of numerical stability consideration, the proposal distribution shall be chosen as $(|\Psi_o(0)[s]|^2 + \sum c_i^2 |\Theta_i[s]|^2)$ in case of very sparse initial condition. As for the orthogonality penalty term, $(|\Theta_i[s]|^2 + |\Theta_j[s]|^2)$ is appropriate to yield a stable estimation. Notice each of the proposal distribution mentioned in this paragraph can be sampled in parallel through l forward propagation.

The loss function presented here is designed to meet the requirements of NAQS on efficient sampling and to avoid local optimum. Thus the fidelity condition is not automatically satisfied, which itself shall not be a problem considering the remarkable fitting ability of deep learning models. The real issue comes from the competition between the noisy estimators of the penalty terms and the down-scaled gradient of the variance loss. This is an intrinsic problem of plain penalty method stuffed with additive penalties. So we plan to reorganize the loss function in the future in order to get rid of any ill-conditioning or local optimum caused by simple-minded penalty method.

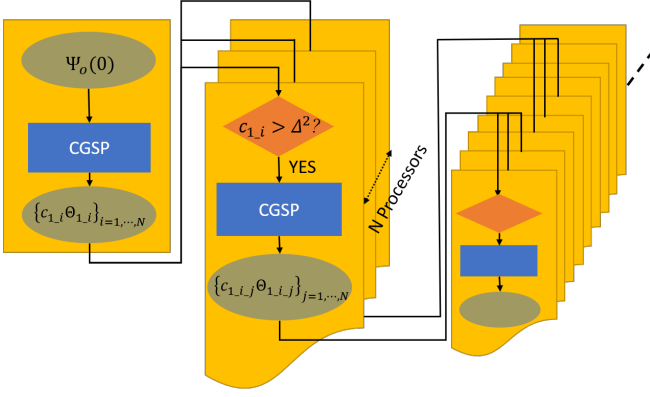


FIG. 1. A parallel scheme for CGSP-breakdown. The label of each states implies a tree structure. $l = 0$ is the root node, $l = 1.i$ is the i -th child of the root node and $l = 1.i.j$ is the j -th child of $l = 1.i$.

C. A parallel framework for CGSP-breakdown

Another important consideration is to avoid optimizing the sum of lots of essentially correlated neural networks simultaneously. To this end, we propose a simple parallel framework for breaking down CGSP into hierarchically-organized sub-tasks. A flowchart of its realization is shown in Fig. 1, where the whole CGSP process is divided into several layers. An initial CGSP of the initial state $\Psi_o(0)$ is carried out in one processor with affordable N . Then the N projected states $\{c_{1,i}\Theta_{1,i}\}$ whose amplitude is above certain threshold Δ are sent to different processors for the next-layer CGSP. Notice the second-step CGSPs are independent and naturally parallel. This procedure can be repeated for higher resolution of the spectrum. At the end, we obtain a family of neural network quantum states organized in a tree structure. All the leaf states can be summed to yield the initial state $\Psi_o(0)$ if CGSP is exact. Otherwise, a supplementary state $(\Psi_o(0) - \sum_{l \in \text{leaf nodes}} c_l \Theta_l)$ should be added to the list of leaf states. To recover the unitary quantum dynamics, the energy expectation λ_l of leaf state labeled by l should be computed for all leaf nodes. The approximation to $\Psi_o(t)$ thus becomes

$$\phi_o(t) = \sum_{l \in \text{leaf nodes}} c_l e^{-i\lambda_l t} \Theta_l. \quad (20)$$

D. Numerical Experiments

We implemented two-layer CGSP closely following the framework presented in this section. As a simple demonstration of practicality, we studied the quench dynamics of 10-spin and 16-spin Heisenberg XXZ chains respectively and compared our results with data from exact diagonalization. For both cases, the Hamiltonian writes $H = \sum_i J(S_i^x S_{i+1}^x + S_i^y S_{i+1}^y + 2S_i^z S_{i+1}^z)$ and the

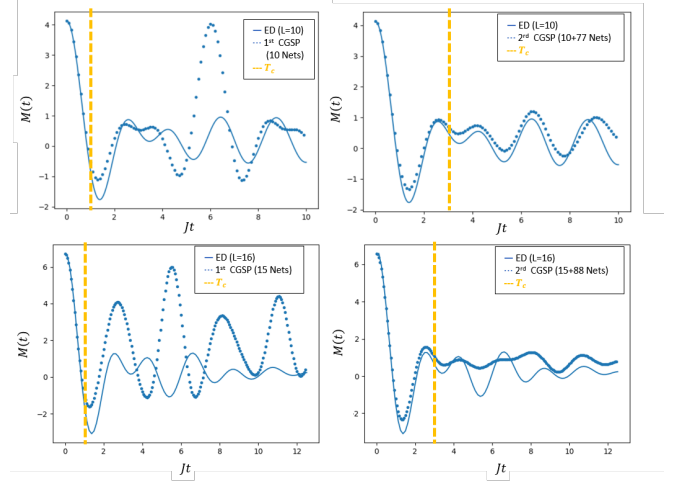


FIG. 2. Dynamical estimation of $M(t)$ after a global quench with or without second-step CGSP. The first row shows the 10-spin XXZ chain results. The second row shows the 16-spin XXZ chain results.

system is quenched from pure states with strong Neel-ordering. Also, both systems are evolving within the half filling sector. The staggered magnetization $M(t) = \sum_i (-1)^i \langle S_i(t) \rangle$ is used to monitor the dynamics.

For 10-spin XXZ chain, the initial CGSP consists of 10 neural networks. 7 of them passed the amplitude test and was sent to 7 NVIDIA V100 GPUs for parallel refined CGSP. With Eq. 12, a rough estimation of the numerical coherence time T_c satisfying $|\Psi_o(T_c) - \phi_o(T_c)| = 0.1$ can be calculated from the training results for predicting the valid region of predicted dynamics. For 16-spin XXZ chain, the initial CGSP consists of 15 neural networks. Each sub-task of second-layer CGSP consists of 11 neural networks. For both experiments, the dynamical estimation of $M(t)$ before and after the second-step CGSP is shown in Fig. 2. Within the coherence time T_c , we found the CGSP results agree well with the results of exact diagonalization.

The numerical experiments displayed several advantages of CGSP. At the same time, they also exposed some serious issues with our current design.

An obvious advantage of CGSP is the predictable coherence time, which gives a rough but useful valid region of the dynamical estimation of the observables. Also, the over-idealized Eq. (7) will provide CGSP practitioners a clear sense of how many neural networks may be needed and how to divide them in a hierarchy way. The actual needed number of networks can be reduced by the parallel scheme we proposed for work-breakdown. Appearing to be merely a workaround, the parallel scheme is actually the best annotation to the underlying idea of CGSP. It extracts useful spectral information from quantum states in a coarse-grained way. Yet the extracted information can be refined systematically to improve the accuracy.

The problems with the current implementation of CGSP are also apparent. The most outstanding issue

is in the optimization. As we have mentioned before, the estimated gradient of the loss Eq. (19) is mainly noise when η_1 is small. So a sluggish gradient descent is expected during the later part of the training process. In our experiments, the first-order optimizer ADAM [58] was used. And it indeed appeared to be slowed or even stuck when the fidelity term was already minimized but the variance loss was not yet optimal. This was the reason why we did not simulate larger systems containing, say $20 \sim 100$ spins.

IV. CONCLUSION

We proposed a new framework, coarse-grained spectral projection, for studying quantum unitary dynamics. CGSP is fundamentally different from traditional VMC methods based on time-dependent variational principles. Spectral information of an initial state associated to the system Hamiltonian is fully exploited to predict future dynamics. Advanced deep learning techniques are used to overcome the entanglement barrier and enhance sampling efficiency. In addition, CGSP is tailored to modern high-performance computing infrastructure due to its natural parallelizability. Though not perfect at the current stage, CGSP is potentially a Swiss Army knife for many quantum dynamic problems because it unfolds the hidden spectral structure of individual quantum state. More meaningful physics are encoded in the CGSP results than conventional VMC results. For example, the results of CGSP can be directly used to study dynamical phase transitions across criticality. Moreover, the projected states coming from the same initial state can be dissected and observed respectively. This is especially helpful for studying the thermalization processes or transport processes.

There are still serious problems with the current implementation of CGSP. The most important one is the design of the loss function. This and other problems will be the topic of future publications.

Appendix A

In an ideal case, the classical ansatz can represent any quantum states faithfully. And we are able to use the objective functions Eq. (13) to effectively control the variance of $\{\Theta_i\}$. To show this, we will use the same nota-

tion $\{\psi_i\}$ to denote an increasingly ordered orthonormal eigen-basis associated to Hamiltonian H as in Eq. (1).

For each Θ_i , its unique eigen-decomposition writes

$$\Theta_i = \sum_{k=0}^{N_h-1} a_k^{(i)} \psi_k \quad (\text{A1})$$

In the same way, the initial condition can be decomposed into

$$\Psi_o(0) = \sum_{k=0}^{N_h-1} b_k \psi_k. \quad (\text{A2})$$

Using L_2 norm as the distance measure, the optimization problem Eq. (13) can be recast into

$$\begin{aligned} & \text{minimize} \quad \sum_{i=0}^{N-1} \sum_{k=0}^{N_h-1} \|c_i a_k^{(i)}\|^2 (E_k - \Lambda_i)^2, \\ & \text{subject to} \quad \sum_{k=0}^{N_h-1} \|b_k - \sum_{i=0}^{N-1} c_i a_k^{(i)}\|^2 = 0, \end{aligned} \quad (\text{A3})$$

Let $g_{i,k} = c_i a_k^{(i)}$, the necessary conditions of the minimizer can be written as

$$g_{i,k}^* (E_k - \Lambda_i)^2 = \mu_k \quad (\text{A4})$$

and

$$b_k - \sum_{i=0}^{N-1} g_{i,k}^* = 0. \quad (\text{A5})$$

In Eq. (A4), μ_k is a multiplier going to be determined. Combining Eq. (A4) and Eq. (A5) yields

$$g_{i,k}^* = \frac{b_i}{\sum_{j=0}^{N-1} \frac{(E_k - \Lambda_i)^2}{(E_k - \Lambda_j)^2}} \quad (\text{A6})$$

To understand Eq. (A6), recall that $\{\Lambda_i\}$ is evenly spaced with distance ϵ . When $(\Lambda_{N-1} - \Lambda_0)$ is fixed and N is large enough, the minimizer Θ_i^* has a nearly N -invariant energy distribution $P((E_k - \lambda_i)/\epsilon) = \|g_{i,k}^*/b_i\|^2$ with a quartic tail. Thus, $\frac{\langle \Theta_i^* | (H - \Lambda_i)^2 | \Theta_i^* \rangle}{\langle \Theta_i^* | \epsilon^2 | \Theta_i^* \rangle}$ is not sensitive to N .

We immediately have the conclusion that $\frac{\langle \Theta_i^* | (H - \Lambda_i)^2 | \Theta_i^* \rangle}{\langle \Theta_i^* | \Theta_i^* \rangle}$ scales with N^{-2} .

-
- [1] A. M. Kaufman, B. J. Lester, and C. A. Regal, *Physical Review X* **2**, 041014 (2012), arXiv:1209.2087.
 - [2] W. D. Phillips, *Reviews of Modern Physics* **70**, 721 (1998).
 - [3] D. S. Weiss and M. Saffman, *Physics Today* **70**, 44 (2017).

- [4] J. B. Spring, B. J. Metcalf, P. C. Humphreys, W. S. Kolthammer, X.-M. Jin, M. Barbieri, A. Datta, N. Thomas-Peter, N. K. Langford, D. Kundys, *et al.*, *Science* **339**, 798 (2013).
- [5] L. M. Vandersypen and I. L. Chuang, *NMR techniques for quantum control and computation* (2004),

- arXiv:0404064 [quant-ph].
- [6] H. Schmitz, R. Matjeschk, C. Schneider, J. Glueckert, M. Enderlein, T. Huber, and T. Schaetz, *Physical Review Letters* **103**, 090504 (2009), arXiv:0904.4214.
 - [7] J. Zhang, G. Pagano, P. W. Hess, A. Kyprianidis, P. Becker, H. Kaplan, A. V. Gorshkov, Z. X. Gong, and C. Monroe, *Nature* **551**, 601 (2017), arXiv:1708.01044.
 - [8] J. Zhang, P. W. Hess, A. Kyprianidis, P. Becker, A. Lee, J. Smith, G. Pagano, I. D. Potirniche, A. C. Potter, A. Vishwanath, N. Y. Yao, and C. Monroe, *Nature* **543**, 217 (2017), arXiv:1609.08684.
 - [9] J. Smith, A. Lee, P. Richerme, B. Neyenhuis, P. W. Hess, P. Hauke, M. Heyl, D. A. Huse, and C. Monroe, *Nature Physics* **12**, 907 (2016), arXiv:1508.07026.
 - [10] M. Gring, M. Kuhnert, T. Langen, T. Kitagawa, B. Rauer, M. Schreitl, I. Mazets, D. A. Smith, E. Demler, and J. Schmiedmayer, *Science* **337**, 1318 (2012).
 - [11] X.-D. Cai, C. Weedbrook, Z.-E. Su, M.-C. Chen, M. Gu, M.-J. Zhu, L. Li, N.-L. Liu, C.-Y. Lu, and J.-W. Pan, *Physical review letters* **110**, 230501 (2013).
 - [12] A. A. Houck, H. E. Türeci, and J. Koch, *Nature Physics* **8**, 292 (2012).
 - [13] T. P. Hartly, D. T. Allcock, C. J. Ballance, L. Guidoni, H. A. Janacek, N. M. Linke, D. N. Stacey, and D. M. Lucas, *Physical Review Letters* **113**, 220501 (2014), arXiv:1403.1524.
 - [14] F. Arute, K. Arya, R. Babbush, D. Bacon, J. C. Bardin, R. Barends, R. Biswas, S. Boixo, F. G. Brandao, D. A. Buell, *et al.*, *Nature* **574**, 505 (2019).
 - [15] J. W. Pan, Z. B. Chen, C. Y. Lu, H. Weinfurter, A. Zeilinger, and M. Zukowski, *Reviews of Modern Physics* **84**, 777 (2012), arXiv:0805.2853.
 - [16] T. B. Wahl, A. Pal, and S. H. Simon, *Physical Review X* **7**, 021018 (2017).
 - [17] T. Devakul and R. R. Singh, *Physical review letters* **115**, 187201 (2015).
 - [18] F. A. Schröder, D. H. Turban, A. J. Musser, N. D. Hine, and A. W. Chin, *Nature Communications* **10**, 1 (2019).
 - [19] R. Khasseh, A. Russomanno, M. Schmitt, M. Heyl, and R. Fazio, *Physical Review B* **102**, 014303 (2020).
 - [20] J. Del Pino, F. A. Schröder, A. W. Chin, J. Feist, and F. J. Garcia-Vidal, *Physical Review Letters* **121**, 227401 (2018), arXiv:1804.04511.
 - [21] A. H. Werner, D. Jaschke, P. Silvi, M. Kliesch, T. Calarco, J. Eisert, and S. Montangero, *Physical Review Letters* **116**, 237201 (2016).
 - [22] P. Doria, T. Calarco, and S. Montangero, *Physical Review Letters* **106**, 190501 (2011).
 - [23] M. Bukov, A. G. Day, D. Sels, P. Weinberg, A. Polkovnikov, and P. Mehta, *Physical Review X* **8**, 031086 (2018), arXiv:1705.00565.
 - [24] M. Y. Niu, S. Boixo, V. N. Smelyanskiy, and H. Neven, *npj Quantum Information* **5**, 1 (2019).
 - [25] K. Wang, X. Qiu, L. Xiao, X. Zhan, Z. Bian, W. Yi, and P. Xue, *Physical Review Letters* **122**, 020501 (2019), arXiv:1806.10871.
 - [26] G. A. Worth, H.-D. Meyer, H. Köppel, L. S. Cederbaum, and I. Burghardt, *International Reviews in Physical Chemistry* **27**, 569 (2008).
 - [27] M. A. Nielsen and I. L. Chuang, *Quantum Computation and Quantum Information* (Cambridge University Press, 2010).
 - [28] J. Preskill, *Quantum* **2**, 79 (2018), arXiv:1801.00862.
 - [29] J. Chiaverini, D. Leibfried, T. Schaetz, M. D. Barrett, R. B. Blakestad, J. Britton, W. M. Itano, J. D. Jost, E. Knill, C. Langer, R. Ozeri, and D. J. Wineland, *Nature* **432**, 602 (2004).
 - [30] S. R. White, *Physical Review Letters* **69**, 2863 (1992).
 - [31] U. Schollwöck, *Annals of Physics* **326**, 96 (2011), arXiv:1008.3477.
 - [32] F. Verstraete, V. Murg, and J. Cirac, *Advances in Physics* **57**, 143 (2008).
 - [33] G. Vidal, *Physical Review Letters* **99**, 220405 (2007), arXiv:0512165 [cond-mat].
 - [34] M. B. Hastings, *Journal of Statistical Mechanics: Theory and Experiment* **2007**, P08024 (2007).
 - [35] S. Bravyi, M. B. Hastings, and F. Verstraete, *Physical Review Letters* **97**, 050401 (2006), arXiv:0603121 [quant-ph].
 - [36] D. L. Deng, X. Li, and S. Das Sarma, *Quantum entanglement in neural network states* (2017), arXiv:1701.04844.
 - [37] G. Carleo and M. Troyer, *Science* **355**, 602 (2017).
 - [38] J. Han, L. Zhang, and E. Weinan, *Journal of Computational Physics* **399**, 108929 (2019).
 - [39] K. Choo, T. Neupert, and G. Carleo, *Physical Review B* **100**, 125124 (2019).
 - [40] D. Pfau, J. S. Spencer, A. G. d. G. Matthews, and W. M. C. Foulkes, *arXiv preprint arXiv:1909.02487* (2019).
 - [41] D. Luo and B. K. Clark, *Physical review letters* **122**, 226401 (2019).
 - [42] J. Hermann, Z. Schätzle, and F. Noé, *arXiv preprint arXiv:1909.08423* (2019).
 - [43] Y. Levine, O. Sharir, N. Cohen, and A. Shashua, *Physical Review Letters* **122**, 065301 (2019), arXiv:1803.09780.
 - [44] K. Choo, A. Mezzacapo, and G. Carleo, *Nature Communications* **11**, 1 (2020), arXiv:1909.12852.
 - [45] M. Schmitt and M. Heyl, *arXiv preprint arXiv:1912.08828* (2019).
 - [46] G. Fabiani and J. Mentink, *arXiv preprint arXiv:1912.10845* (2019).
 - [47] M. J. Hartmann and G. Carleo, *Physical review letters* **122**, 250502 (2019).
 - [48] R. L. Kosut, T.-S. Ho, and H. Rabitz, *arXiv preprint arXiv:2006.13498* (2020).
 - [49] O. Sharir, Y. Levine, N. Wies, G. Carleo, and A. Shashua, *Physical Review Letters* **124**, 020503 (2020), arXiv:1902.04057.
 - [50] F. Alet and N. Laflorencie, *Many-body localization: An introduction and selected topics* (2018), arXiv:1711.03145.
 - [51] T. B. Wahl, A. Pal, and S. H. Simon, *Physical Review X* **7**, 021018 (2017).
 - [52] S. Czischek, M. Gärttner, and T. Gasenzer, *Physical Review B* **98**, 024311 (2018), arXiv:1803.08321.
 - [53] A. Paszke, S. Gross, F. Massa, A. Lerer, J. Bradbury, G. Chanan, T. Killeen, Z. Lin, N. Gimelshein, L. Antiga, *et al.*, in *Advances in neural information processing systems* (2019) pp. 8026–8037.
 - [54] M. Abadi, A. Agarwal, P. Barham, E. Brevdo, Z. Chen, C. Citro, G. S. Corrado, A. Davis, J. Dean, M. Devin, *et al.*, *arXiv preprint arXiv:1603.04467* (2016).
 - [55] A. v. d. Oord, S. Dieleman, H. Zen, K. Simonyan, O. Vinyals, A. Graves, N. Kalchbrenner, A. Senior, and K. Kavukcuoglu, *arXiv preprint arXiv:1609.03499* (2016).
 - [56] A. Bansal, X. Chen, B. Russell, A. Gupta, and D. Ramanan, *arXiv preprint arXiv:1609.06694* (2016).

- [57] A. Van Den Oord, N. Kalchbrenner, O. Vinyals, L. Espeholt, A. Graves, and K. Kavukcuoglu, in *Advances in Neural Information Processing Systems* (2016) pp. 4797–4805, arXiv:1606.05328.
- [58] D. P. Kingma and J. Ba, arXiv preprint arXiv:1412.6980 (2014).